North Atlantic ocean circulation and abrupt climate change during the last glaciation

Authors: L. G. Henry[1*], J. F. McManus[1], W. B. Curry[2,3], N. L. Roberts[4], A. M. Piotrowski[4], L. D. Keigwin[2]

[1]Lamont-Doherty Earth Observatory, Columbia University, Palisades, NY 10964 USA.

[2] Woods Hole Oceanographic Institution, Woods Hole, MA 02543. USA

[3] Bermuda Institute of Ocean Sciences, St. George's, Bermuda.

[4] University of Cambridge, Department of Earth Sciences, Cambridge UK CB2 3EQ

*Author to whom correspondence should be addressed (lhenry@ldeo.columbia.edu)

The most recent ice age was characterized by rapid and hemispherically asynchronous climate oscillations, whose origin remains unresolved. Variations in oceanic meridional heat transport may contribute to these repeated climate changes, which were most pronounced during the glacial interval twenty-five to sixty thousand years ago known as marine isotope stage 3 (MIS3). Here we examine a sequence of climate and ocean circulation proxies throughout MIS3 at high resolution in a deep North Atlantic sediment core, combining the kinematic tracer Pa/Th with the most widely applied deep water-mass tracer, $\delta^{13}C_{BF}$. These indicators reveal that Atlantic overturning circulation was reduced during every cool northern stadial, with the greatest reductions during episodic iceberg discharges from the Hudson Strait, and that sharp northern warming followed reinvigorated overturning. These results provide direct evidence for the ocean's persistent, central role in abrupt glacial climate change.

One Sentence Summary: Multiple proxies reveal that ocean circulation changes accompanied and preceded each millennial climate oscillation within marine isotope stage 3 (MIS 3) of the most recent ice age, 60ka to 25ka.

Unlike the relatively stable preindustrial climate of the past ten thousand years, glacial climate was characterized by repeated millennial oscillations (*1*). These alternating cold stadial and warm interstadial events were most abrupt and pronounced on Greenland and across much of the northern hemisphere, with the most extreme regional conditions during several Heinrich (H) events (*2*), catastrophic iceberg discharges into the subpolar North Atlantic Ocean. These abrupt events not only had impact on global climate, but also are associated with widespread reorganizations of the planet's ecosystems(*3*). Geochemical fingerprinting of the ice rafted detritus (IRD) associated with the most pronounced of these events consistently indicates a source in the Hudson Strait (HS) (*4*), so we abbreviate this subset of H events as HS events and their following cool periods as HS stadials. During northern stadials, ice cores show that Antarctica warmed, and each subsequent rapid northern hemisphere warming was followed shortly by cooling at high southern latitudes (*5*). Explanations for the rapidity and asynchrony of these climate changes require a mechanism for partitioning heat on a planetary scale, initiated either through reorganization of atmospheric structure (*6*) or the ocean's thermohaline circulation, particularly the Atlantic meridional overturning circulation (AMOC) (*7-10*). Coupled climate models have successfully used each of these mechanisms to generate time series that replicate climate variability observed in paleoclimate archives (*9*, *11*). Here we investigate the relationship between Northern

Hemispheric climate as recorded in Greenland ice cores and marine sediments, along with isotopic deep-sea paleoproxies sensitive to changes in North Atlantic Deep Water (NADW) production and AMOC transport during MIS3. Throughout that time, when climate was neither as warm as today nor as cold as the last glacial maximum (LGM), ice sheets of intermediate size blanketed much of the northern hemisphere, and large millennial stadial - interstadial climate swings (*6*, *8*) provide a wide dynamic range that allows examination of the ocean's role in abrupt change.

Sediment samples were taken from the long (35m) core KNR191-CDH19, recovered from the Bermuda Rise (33˚ 41.443' N; 57˚ 34.559' W, 4541m water depth) in the northwestern Atlantic Ocean (Fig. 1), near previous seafloor sampling at Integrated Ocean Drilling Program (IODP) site 1063, and coring sites KNR31 GPC-5, EN120 GGC-1, MD95-2036, and others. Because this region of the deep North Atlantic is characterized by steep lateral gradients in tracers of NADW and Antarctic Bottom Water (AABW), the Bermuda Rise has been intensively used to explore the connection between changes in ocean circulation and climate (*7, 12*). In this study we measured the radioisotopes ^{231}Pa and ^{230}Th in bulk sediment, age-corrected to the time of deposition, along with stable carbon (δ^{13}C) and oxygen (δ^{18}O) isotope ratios in the microfossil shells of both epibenthic foraminifera (*Cibicidoides wuellerstorfi* and *Nuttallides umbonifera)* and planktonic foraminifera (*Globergerinoides ruber)* respectively, yielding inferences on relative residence times and the origin of deep water masses on centennial time scales.

The isotopes ^{231}Pa and ^{230}Th are produced from the decay of ^{235}U and ^{234}U, respectively, dissolved in seawater. This activity of ^{231}Pa and ^{230}Th in excess of the amount supported by the decay of uranium within the crystal lattice of the sediment's mineral grains is denoted by $^{231}P_{xs}$ and $^{230}Th_{xs}$. As the parent U isotopes have long residence times, U is well mixed throughout the ocean. This yields a $^{231}Pa_{xs}/^{230}Th_{xs}$ (hereafter Pa/Th) production ratio (Pa/Th = 0.093) that is constant and uniformly distributed (*13*, *14*). Both daughter isotopes are removed by adsorption onto settling particles, with Th more efficiently scavenged than Pa. The residence time of $^{231}Pa_{xs}$ (τ_{res} ~= 200yr) in seawater is thus greater than that of $^{230}Th_{xs}$ (τ_{res} ~= 30yr), allowing $^{231}Pa_{xs}$ to be redistributed laterally by changes in basin-scale circulation before deposition (*7*, *14*-*16*), with the additional potential influence of removal due to changes in particle rain associated with biological productivity (*17*). Settling particles (*18*) and surface sediments throughout the basin reveal a deficit in $^{231}Pa_{xs}$ burial that is consistent with large-scale export by the deep circulation (Fig. 1 and supplemental discussion).

The downcore Pa/Th in core CDH-19 ranges from ~0.05 to slightly above the production ratio of 0.093, with a series of well-defined variations throughout MIS 3 (Fig.2). In sediments deposited during Greenland interstadial intervals(*1*), Pa/Th ratios average 0.0609+/-0.0074 (2σ), substantially below the production ratio (Fig. 2), and only 10% higher than the mean value (Pa/Th = 0.055) of the Holocene, a time of relatively vigorous AMOC (*7*). Because $^{230}Th_{xs}$ is buried in near balance with its production (*19*), the relatively low Pa/Th indicates a substantial lateral export of $^{231}Pa_{xs}$, consistent with relatively vigorous AMOC during interstadials, although the vertical integration through the water column of this deficit does not distinguish whether this export occurred at deep or intermediate levels. Epibenthic $\delta^{13}C$ ($\delta^{13}C_{BF}$) data allow discrimination between these two possibilities, and display increased values during each interstadial, implying a greater contribution of the isotopically more positive North Atlantic end member (Fig 2). During these intervals, this positive isotopic signal suggests a deeper overturning cell was established, rather than a shallower, yet vigorous one. This confirms a previous suggestion of intervals of relatively strong AMOC within the most recent ice age (*20*, *21*), although neither Pa/Th nor $\delta^{13}C_{BF}$ adjusted for whole ocean inventory changes (*22*) reach early Holocene values.

Pa/Th increases within each Greenland stadial interval, for a mean duration of 0.531 +/- 0.303ka to a Pa/Th value of 0.0797+/-0.0154, indicating decreased lateral export of $^{231}Pa_{xs}$ and consistent with a shallower or reduced overturning cell in the North Atlantic. During these stadials, $\delta^{13}C_{BF}$ decreases substantially to negative values (-0.2‰ to -0.5‰), suggesting greater influence of the glacial equivalent of modern Antarctic Bottom Water (AABW), an isotopic result consistent with reduced AMOC from a coupled climate model (*10*). Although the northern and southern water mass end members are not well known throughout the most recent glaciation, deep waters in the Atlantic during the LGM ranged from less than -0.5‰ in the south to more than 1.5‰ in the north (*22*). If these values prevailed throughout MIS 3, then the low benthic $\delta^{13}C_{BF}$ indicates a dominant stadial influence of southern waters, and substantial northward retreat or shoaling of the AABW/NADW mixing zone, which is consistent with the deep water mass configuration that has previously been reconstructed for the LGM (*22*, *23*), although not for millennial-scale stadial intervals within the glaciation.

The mean Pa/Th of both stadials and interstadials is consistent with export of $^{231}Pa_{xs}$ from the subtropical North Atlantic during all of MIS3. During peak interstadials, when low Pa/Th indicates the local burial of approximately half of $^{231}Pa_{xs}$ production, the remaining half would have been exported. In contrast, the substantial decrease in the lateral export of $^{231}Pa_{xs}$ evident in higher Pa/Th, along with lower benthic $\delta^{13}C_{BF}$ during each stadial interval, points to repeated reductions in AMOC and its attendant northward heat transport throughout MIS3. The contrast between apparent deep, vigorous overturning during interstadials, with shallower(*24*), weaker overturning during stadials, is most pronounced in conjunction with all HS stadials (Fig. 2), when catastrophic discharge of melting icebergs from Canada flooded the subpolar North Atlantic (*4*).

Sediments deposited during HS stadials are characterized by a mean duration of 1.65 +/- 0.545ka and an average Pa/Th of 0.095 +/- 0.016, which is indistinguishable from the production ratio. These results therefore indicate no net export of $^{231}Pa_{xs}$ from the subtropical North Atlantic during these events sourced from the Hudson Strait. This balance between seawater radiometric production and underlying sedimentary burial would be expected under conditions with a substantial reduction in AMOC or other lateral transport, and might imply a near cessation of $^{231}Pa_{xs}$ export through deep circulation. Although variable scavenging may also contribute to sedimentary Pa/Th, values throughout MIS 3 bear only a weak relationship with bulk and opal fluxes (r^2=0.19, S2), which therefore constitute secondary influences.

These new results reveal that AMOC variations were associated with every MIS 3 stadial-interstadial oscillation, with the largest reductions during HS stadials. The well-resolved interval 35-50 ka provides a good example (Fig. 3). This iconic interval contains H4, H5, and the intervening series of oscillations that have served as a basis for conceptual and computer models seeking to explain such variability (*8-11*, *25*, *26*). A previous Pa/Th record (*20*) covering this interval captured much of the overall amplitude, and the new data resolve each stadial increase in Pa/Th, indicating that only HS4 and

HS5 reach the production ratio of 0.093. Because the interstadial values are similar to each other, the subsequent abrupt increases in AMOC and regional warming are also the greatest, and occur within the century-scale response time of Pa/Th. Throughout the records, the Pa/Th and $\delta^{13}C_{BF}$ bear a striking similarity to model output forced by freshwater anomalies (*11*).

Combined with previous investigations (*7*, *27*), these new results confirm that all HS events of the past 60kyr were associated with a dramatic increase in Pa/Th, and are evidence for major reduction in AMOC in association with the largest IRD events (*28*). In contrast, H3, the sole Heinrich event stadial that fails to reach the production ratio (peak Pa/Th = 0.079), displays smaller IRD fluxes across the subpolar Atlantic (*28*) with provenance inconsistent with a Hudson Strait source (*4*). This muted result for H3 is consistent with evidence from the Florida Straits (*29*) showing a smaller reduction at that time in the northward flow of near-surface waters that feed the overturning circulation. As with all stadials, the HS events are characterized by lower $\delta^{13}C_{BF}$, suggesting diminished influence of NADW and proportionately greater AABW on Bermuda Rise. Combined Pa/Th and $\delta^{13}C_{BF}$ results therefore indicate a persistent pattern of stadial weakening and interstadial strengthening, with a repeatedly largest reduction in AMOC associated with all HS events. Although these observations are consistent with a number of numerical model simulations (*11*, *26*) as well as conceptual models for the mechanisms of abrupt change, they have previously been difficult to document and fully resolve.

Recent data from the Western Antarctic ice sheet provide compelling evidence for a robust lead of Greenland climate over Antarctica (*5*). That analysis revealed a N.

Hemisphere lead of 208 +/-96 years, indicating that the interhemispheric teleconnection propagates from north to south on timescales consistent with basin-scale ocean circulation. To ascertain whether Northern Hemisphere climate is forced or reinforced by changes in AMOC, we investigated the phase relationship between surface and deep-sea properties. Cross-correlations were performed on each of $\delta^{13}C_{BF}$, Pa/Th, SST, $CaCO_3$ with NGRIP $\delta^{18}O$ from both sediment cores CDH19 and MD95-2036 from the Bermuda Rise. The optimal correlation of $\delta^{13}C_{BF}$ leads NGRIP $\delta^{18}O$ by approximately two centuries (Fig 4). This lead is corroborated by Pa/Th phasing which, when considering the century-scale response time of the proxy (*13*, *14*), is consistent with AMOC changes indicated by $\delta^{13}C_{BF}$. The SST reconstruction from MD95-2036 was aligned with Greenland $\delta^{18}O$, yielding a correlation of r^2=0.83(*30*). SST and Pa/Th are synchronous with NGRIP to within the estimated bioturbation error of 8cm within the core, displaying correlations with Greenland of r^2 =0.47 for Pa/Th, and r^2 =0.65 for SST. The optimal correlation of %$CaCO_3$, r^2 =0.64, lags NGRIP $\delta^{18}O$ by nearly 200 years.

The consistent lead of variations in $\delta^{13}C_{BF}$ before SST and Greenland temperatures, repeated over multiple millennial cycles, indicates the potential influence of AMOC on NH climate, and suggests the Bermuda Rise is exposed to shifts in deep water mass mixing. Initially, deep circulation changes, evidenced overall by the timing of $\delta^{13}C_{BF}$. Pa/Th shifts are essentially in tandem with regional temperature when circulation accelerates, and soon thereafter as it responds to weakening AMOC (S3). Given the response time of Pa/Th to instantaneous shifts in North Atlantic overturning(*13*, *14*), this also suggests that changes in AMOC precede regional temperature change, although the exact timing may have differed during cooling and warming phases. Both SST and

Greenland temperature proxies lag the ocean circulation in a consistent fashion, and in turn these northern changes have been demonstrated to lead Antarctic temperatures (*5*). Calcium-carbonate concentration is the last of the proxies to respond to AMOC change, consistent with the longer timescale of preservation, dissolution and dilution in the deep ocean.

The relative timing of the observed AMOC changes has important implications for regional and global climate. While numerous computer simulations suggest that melting icebergs and other freshwater input associated with H events may have shut down NADW production(*9*, *11*, *26*), recent results examining the phasing of North Atlantic SST and ice rafted detritus (IRD) suggest stadial conditions began to develop prior to ice-rafting(*31*). The evidence here nevertheless indicates that the greatest AMOC reduction and the coldest stadial intervals accompanied the largest iceberg discharges. This suggests that the iceberg discharges may have provided a positive feedback mechanism to accelerate the initial cooling within each multi millennial climate cycle. In addition, the extended Heinrich-stadial reductions in AMOC observed in this study coincide with intervals of rising atmospheric CO_2(*32*), while CO_2 declined when AMOC increased during the subsequent sharp transitions to northern interstadials, supporting a potential influence on the atmosphere by the deep circulation on millennial timescales(*33*).

The robust relationship of reductions in export of northern deep waters evident in reduced $^{231}Pa_{xs}$ export and decreased $\delta^{13}C_{BF}$ before and during stadial periods, and the dramatic increases in both during interstadials provides direct evidence for the role of AMOC in abrupt glacial climate change. The sequence of marked circulation changes and northern hemisphere climate detailed here, combined with the demonstrated lag of Antarctic temperature variations (*5*), strongly implicates changes in meridional heat transport by the ocean as a trigger for abrupt northern hemisphere warming and the tipping of the "bipolar seesaw (*25*)."

Figures

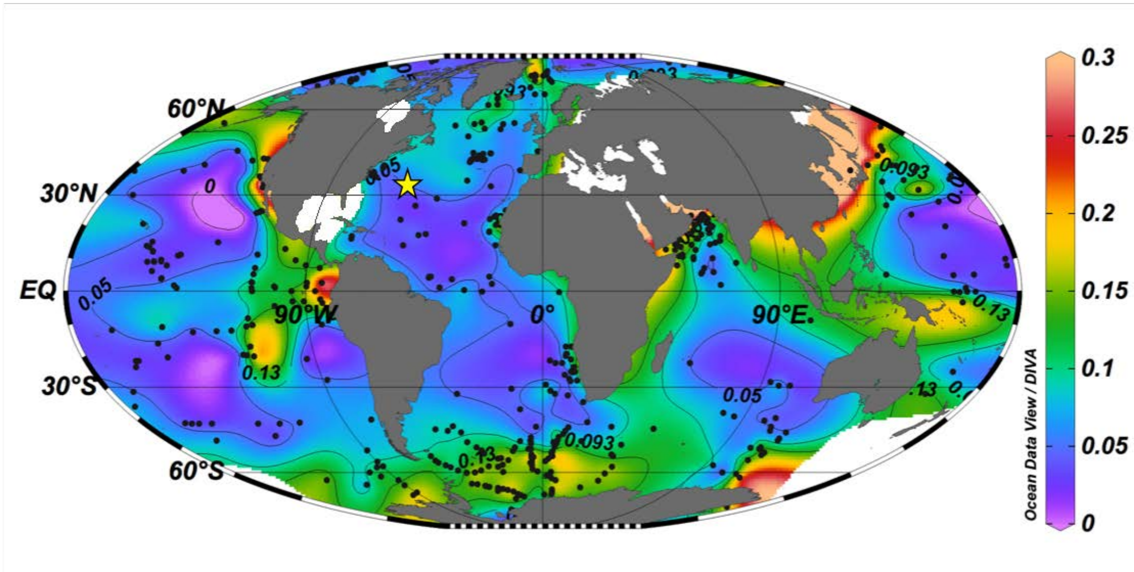

Fig. 1. Location sediment core CDH19 shown as star (33˚ 41.443’ N; 57˚ 34.559’ W, 4541m water depth) with Pa/Th ratios (black dots) in core top sediments used with ODV DIVA gridding to produce the color contours. White areas contain no data.

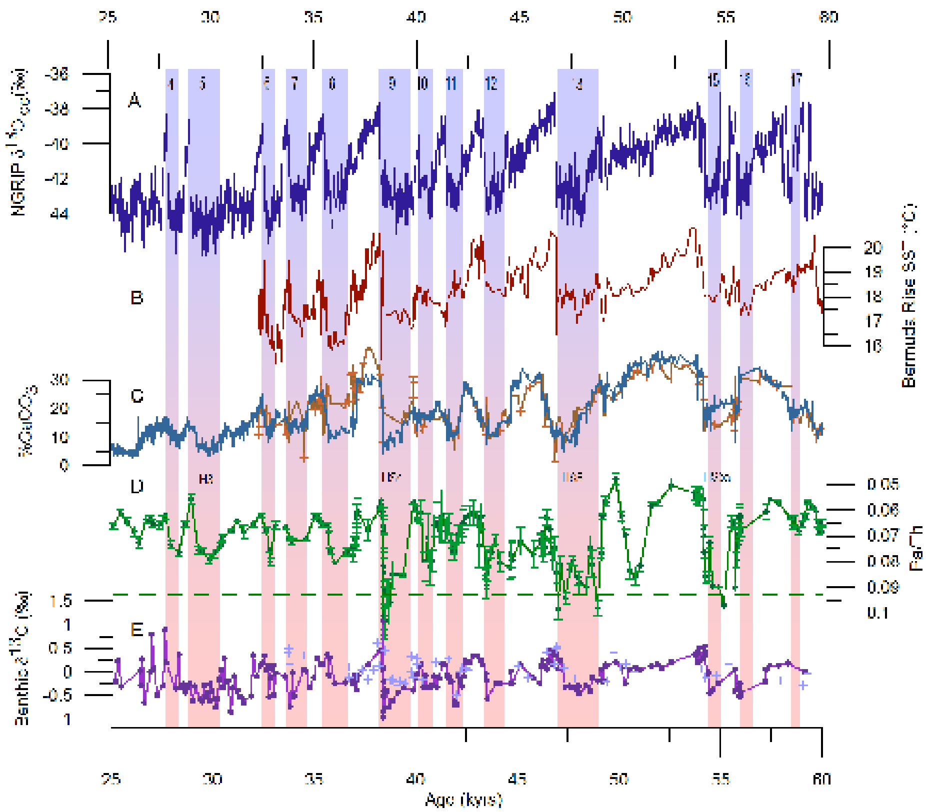

Fig. 2. Stadials are numbered with vertical bars. [A] NGRIP ice core $\delta^{18}O_{ice}$ 75.1°N, 42.32°W (*34*). [B] SST (°C) from MD95-2036, 33˚ 41.444'N, 57˚ 34.548'W, 4462m (*30*). [C] Calcium x-ray fluorescence (orange) from core CDH19 (this study) mapped to $\%CaCO_3$, with calibration $r^2 = 0.87$ (S.1), with spectral reflectance (blue) from core MD95-2036 (*35*) [D] Pa/Th from bulk sediment (green) taken from core CDH19. [G] Benthic foraminiferal $\delta^{13}C_{BF}$ from core CDH19 (purple) alternates between values consistent with southern and northern sourced $\delta^{13}C_{BF}$ end members.

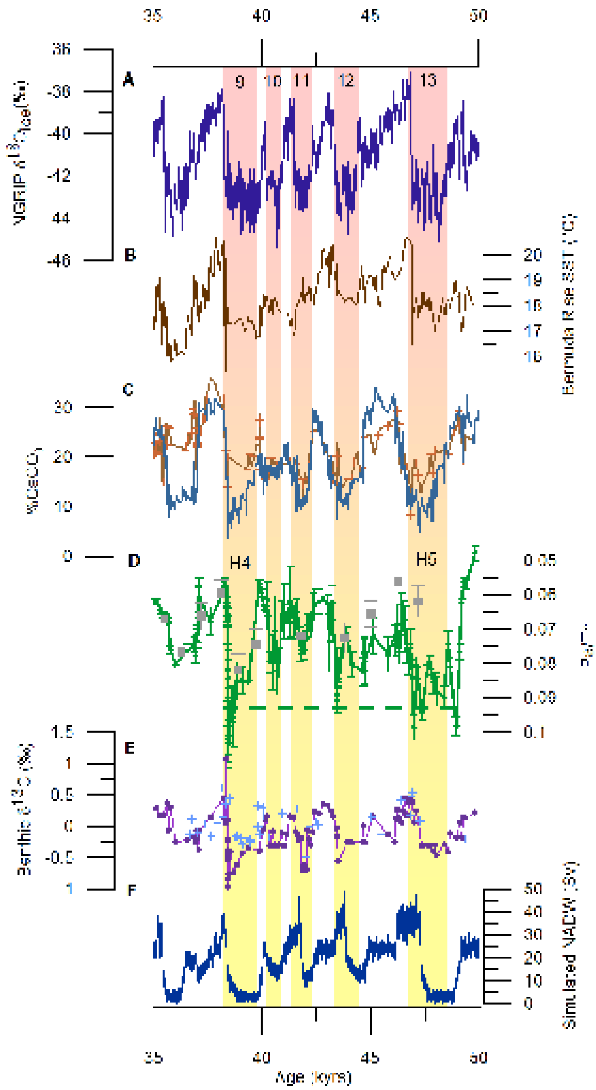

Fig. 3. (A) through (E) as in Figure 2, with the addition of (F) simulated NADW (Sv) in a coupled ocean/atmosphere model (*11*), with previously published Böhm et al Pa/Th data (*20*) and Keigwin and Boyle $\delta^{13}C_{BF}$ data (*12*).

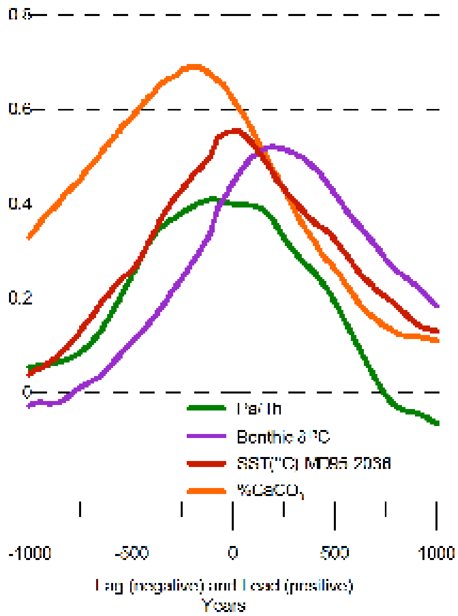

Fig. 4. Correlation of NGRIP ice core $\delta^{18}O$ with CDH19 $\%CaCO_3$ (orange), Pa/Th of bulk sediment from CDH19 (green), $\delta^{13}C_{BF}$ from CDH19 (purple), SST °C from MD95-2036 (*30*) (red).

References and Notes

1. W. Dansgaard, S. Johnsen, H. Clausen, Evidence for general instability of past climate from a 250-kyr ice-core record. *Nature*. **364**, 218–220 (1993).

2. W. Broecker, G. Bond, M. Klas, E. Clark, J. McManus, Origin of the northern Atlantic's Heinrich events. *Climate Dynamics*. **6**, 265–273 (1992).

3. M. Yasuhara, T. M. Cronin, P. B. Demenocal, H. Okahashi, B. K. Linsley, Abrupt climate change and collapse of deep-sea ecosystems. *Proceedings of the National Academy of Sciences of the United States of America*. **105**, 1556–1560 (2008).

4. S. R. Hemming, Heinrich events: Massive late Pleistocene detritus layers of the North Atlantic and their global climate imprint. *Rev. Geophys.* **42** (2004).

5. C. Buizert *et al.*, Precise interpolar phasing of abrupt climate change during the last ice age. *Nature*. **520**, 661–665 (2015).

6. X. Zhang, G. Lohmann, G. Knorr, C. Purcell, Abrupt glacial climate shifts controlled by ice sheet changes. *Nature*. **512**, 290–294 (2014).

7. J. McManus, R. Francois, J. M. Gherardi, L. Keigwin, S. Brown-Leger, Collapse and rapid resumption of Atlantic meridional circulation linked to deglacial climate changes. *Nature*. **428**, 834–837 (2004).

8. R. B. Alley, P. Clark, L. Keigwin, R. Webb, Making sense of millennial-scale climate change. *Geoph Monog Series*. **112**, 385–394 (1999).

9. S. Rahmstorf, Ocean circulation and climate during the past 120, 000 years. *Nature*. **419**, 207–214 (2002).

10. A. Schmittner, D. C. Lund, Early deglacial Atlantic overturning decline and its role in atmospheric CO_2 rise inferred from carbon isotopes ($\delta^{13}C$). *Clim Past*. **11**, 135–152 (2015).

11. L. Menviel, A. Timmermann, T. Friedrich, Hindcasting the continuum of Dansgaard-Oeschger variability: mechanisms, patterns and timing. *Clim Past* (2013).

12. L. Keigwin, E. Boyle, Surface and deep ocean variability in the northern Sargasso Sea during marine isotope stage 3. *Paleoceanography* (1999).

13. G. M. Henderson, R. F. Anderson, The U-series toolbox for paleoceanography. *Rev mineral geochem*. **52**, 493 (2003).

14. E. F. Yu, R. Francois, M. P. Bacon, Similar rates of modern and last-glacial ocean thermohaline circulation inferred. *Nature*. **379**, 22 (1996).

15. C. Negre *et al.*, Reversed flow of Atlantic deep water during the Last Glacial Maximum. *Nature*. **468**, 84–88 (2010).

16. J. M. Gherardi *et al.*, Glacial–interglacial circulation changes inferred from $^{231}Pa/^{230}Th$ sedimentary record in the North Atlantic region. *Paleoceanography*. **24** (2009).

17. R. F. Anderson *et al.*, Wind-Driven Upwelling in the Southern Ocean and the Deglacial Rise in Atmospheric CO_2. *Science*. **323**, 1443–1448 (2009).

18. C. Hayes, R. F. Anderson, M. Fleisher, S. Vivancos, Intensity of Th and Pa scavenging partitioned by particle chemistry in the North Atlantic Ocean. *Mar Chem*. **170**, 49–60 (2015).

19. G. M. Henderson, C. Heinze, R. F. Anderson, A. M. E. Winguth, Global distribution of the ^{230}Th flux to ocean sediments constrained by GCM modelling. *Deep Sea Res PT I*. **46**, 1861–1893 (1999).

20. E. Böhm *et al.*, Strong and deep Atlantic meridional overturning circulation during the last glacial cycle. *Nature*. **517**, 73–76 (2014).

21. J. Gottschalk *et al.*, Abrupt changes in the southern extent of North Atlantic Deep Water during Dansgaard–Oeschger events. *Nat Geosci*. **8**, 950–954 (2015).

22. W. B. Curry, D. W. Oppo, Glacial water mass geometry and the distribution of $\delta^{13}C$ of ΣCO_2 in the western Atlantic Ocean. *Paleoceanography*. **20** (2005).

23. J. F. Adkins, The role of deep ocean circulation in setting glacial climates. *Paleoceanography*. **28**, 539–561 (2013).

24. R. Zahn, A. Stüber, Suborbital intermediate water variability inferred from paired benthic foraminiferal Cd/Ca and $\delta^{13}C$ in the tropical West Atlantic and linking with North Atlantic climates. *Earth Planet Sc Lett*. **200**, 191–205 (2002).

25. W. Broecker, Paleocean circulation during the last deglaciation: a bipolar seesaw? *Paleoceanography*. **13**, 119–121 (1998).

26. A. Ganopolski, S. Rahmstorf, Rapid changes of glacial climate simulated in a coupled climate model. *Nature*. **409**, 153–158 (2001).

27. J. Lippold *et al.*, Does sedimentary $^{231}Pa/^{230}Th$ from the Bermuda Rise monitor past Atlantic Meridional Overturning Circulation? *Geophys. Res. Lett.* **36** (2009).

28. J. F. McManus, R. F. Anderson, W. S. Broecker, M. Q. Fleisher, S. M. Higgins, Radiometrically determined sedimentary fluxes in the sub-polar North Atlantic during the last 140,000 years. *Earth Planet Sc Lett*. **155**, 29–43 (1998).

29. J. Lynch-Stieglitz, M. Schmidt, L. Henry, W. B. Curry, Muted change in Atlantic

overturning circulation over some glacial-aged Heinrich events. *Nat Geosci*. **7**, 144–150 (2014).

30. J. P. Sachs, Subtropical North Atlantic Temperatures 60,000 to 30,000 Years Ago. *Science*. **286**, 756–759 (1999).

31. S. Barker *et al.*, Icebergs not the trigger for North Atlantic cold events. *Nature*. **520**, 333–336 (2015).

32. J. S. Ahn, E. J. Brook, Atmospheric CO2 and Climate on Millennial Time Scales During the Last Glacial Period. *Science*. **322**, 83–85 (2008).

33. A. Schmittner, E. D. Galbraith, Glacial greenhouse-gas fluctuations controlled by ocean circulation changes. *Nature*. **456**, 373–376 (2008).

34. A. Svensson *et al.*, A 60,000 year Greenland stratigraphic ice core chronology. *Clim Past*. **4**, 47–57 (2008).

35. E. Boyle, Characteristics of the deep ocean carbon system during the past 150,000 years: Σ CO2 distributions, deep-water flow patterns, and abrupt climate change. *P Natl Acad Sci USA* **94**, pp. 8300–8307 (1997).

36. R. F. Anderson, M. P. Bacon, P. Brewer, Removal of ^{230}Th and ^{231}Pa at ocean margins. *Earth Planet Sc Lett*. **66**, 73–90 (1983).

37. J. Lippold, S. Mulitza, G. Mollenhauer, S. Weyer, Boundary scavenging at the East Atlantic margin does not negate use of ^{231}Pa/^{230}Th to trace Atlantic overturning. *Earth Planet Sc Lett*. **333**, 317-331 (2012).

38. F. Deng, A. L. Thomas, M. J. A. Rijkenberg, G. M. Henderson, Controls on seawater ^{231}Pa, ^{230}Th and ^{232}Th concentrations along the flow paths of deep waters in the Southwest Atlantic. *Earth Planet Sc Lett*. **390**, 93–102 (2014).

39. C. T. Hayes *et al.*, ^{230}Th and ^{231}Pa on GEOTRACES GA03, the U.S. GEOTRACES North Atlantic transect, and implications for modern and paleoceanographic chemical fluxes. *Deep-Sea Res Pt Ii*. **116**, 29–41 (2015).

40. R. G. Fairbanks *et al.*, Radiocarbon calibration curve spanning 0 to 50,000 years BP based on paired ^{230}Th/^{234}U/^{238}U and ^{14}C dates on pristine corals. *Quaternary Sci Revs*. **24**, 1781–1796 (2005).

41. D. Yuan, Timing, Duration, and Transitions of the Last Interglacial Asian Monsoon. *Science*. **304**, 575–578 (2004).

42. G. Mollenhauer, M. Kienast, F. Lamy, An evaluation of ^{14}C age relationships between co-occurring foraminifera, alkenones, and total organic carbon in continental margin sediments. *Paleoceanography*. **20** (2005).

43. C. Barbante *et al.*, One-to-one coupling of glacial climate variability in Greenland and Antarctica. *Nature*. **444**, 195–198 (2006).

44. K. K. Andersen *et al.*, High-resolution record of Northern Hemisphere climate extending into the last interglacial period. *Nature*. **431**, 147–151 (2004).

45. W. B. Curry, J. Duplessy, L. Labeyrie, Changes in the distribution of $\delta^{13}C$ of deep water ΣCO2 between the Last Glaciation and the Holocene. *Paleoceanography* (1988).

46. J. C. Duplessy *et al.*, Deepwater source variations during the last climatic cycle and their impact on the global deepwater circulation. *Paleoceanography*. **3**, 343–360 (1988).

47. C. D. Peterson, L. E. Lisiecki, J. V. Stern, Deglacial whole-ocean $\delta^{13}C$ change estimated from 480 benthic foraminiferal records. *Paleoceanography*. **29**, 549–563 (2014).

48. A. Martínez-García *et al.*, Iron Fertilization of the Subantarctic Ocean During the Last Ice Age. *Science*. **343**, 1347–1350 (2014).

49. A. Schmittner *et al.*, Biology and air-sea gas exchange controls on the distribution of carbon isotope ratios ($\delta^{13}C$) in the ocean. *Biogeosciences*. **10**, 5793–5816 (2013).

50. D. M. Sigman, M. P. Hain, G. H. Haug, The polar ocean and glacial cycles in atmospheric CO_2 concentration. *Nature*. **466**, 47–55 (2010).

51. M. Bender, T. Sowers, L. Labeyrie, The Dole effect and its variations during the last 130,000 years as measured in the Vostok ice core. *Global Biogeochem. Cy*. **8**, 363–376 (1994).

52. J. P. Severinghaus, R. Beaudette, M. A. Headly, K. Taylor, E. J. Brook, Oxygen-18 of O_2 Records the Impact of Abrupt Climate Change on the Terrestrial Biosphere. *Science*. **324**, 1431–1434 (2009).

53. N. Shackleton, M. Hall, E. Vincent, Phase relationships between millennial-scale events 64,000-24,000 years ago. *Paleoceanography*. **15**, 565–569 (2000).

54. L. Keigwin, G. Jones, Western North Atlantic evidence for millennial-scale changes in ocean circulation and climate. *J. Geophys. Res* (1994).

Acknowledgements

Data will be made available at http://nsidc. org/data/ and http://ncdc.noaa.gov/paleo/.

This research was supported in part by a NSF Graduate Research Fellowship to L.G.H, by awards from the Comer Science and Education Foundation and NSF ATM-0936496 to J.F.M., and an award from the LDEO Climate Center to L.G.H. and J.F.M. LDK and WBC were supported by ATM-0836472, and LDK was supported by AGS 1548160. We thank M. Jeglinski and K. Rose for technical support. The authors would like to thank R. Anderson, S. Hemming and C. Hayes for constructive discussion leading to improvement of the manuscript, and R. Anderson for unpublished data included in the map figure, and Martin Fleisher for analytical support.